Roller element bearing acoustic fault detection using smartphone and consumer microphones

Comparing with vibration techniques

Jarek Grebenik*, Yu Zhang, Chris Bingham and Saket Srivastava
* The University of Lincoln, School of Engineering, Brayford Pool, Lincoln, LN6 7TS, UK
e-mail: {jgrebenik, yzhang, cbingham, ssrivastava}@lincoln.ac.uk

***Abstract*—Roller element bearings are a common component and crucial to most rotating machinery; their failure makes up around half of the total machine failures, each with the potential to cause extreme damage, injury and downtime. Fault detection through condition monitoring is of significant importance. This paper demonstrates bearing fault detection using widely accessible consumer audio tools. Audio measurements from a smartphone and a standard USB microphone, and vibration measurements from an accelerometer are collected during tests on an electrical induction machine exhibiting a variety of mechanical bearing anomalies. A peak finding method along with use of trained Support Vector Machines (SVMs) classify the faults. It is shown that the classification rate from both the smartphone and the USB microphone was 95 and 100%, respectively, with the direct physically detected vibration results achieving only 75% classification accuracy. This work opens up the opportunity of using readily affordable and accessible acoustic diagnosis and prognosis for early mechanical anomalies on rotating machines.**

Keywords – roller element bearing; acoustic; fault; defect; detection; diagnosis; smartphone; consumer; microphone; vibration; motor; comparison; machine learning; support vector machine; SVM

Abbreviations: AE – Acoustic Emission, ANN – Artificial Neural Network, SVM – Support Vector Machine

I. INTRODUCTION

All rotating machines employ a method of supporting and reducing friction on the rotating shaft. The vast majority use roller element bearings due to their excellent operational performance. As a component vital to smooth operation, their failure can cause extreme damage to other machine components, prolonged downtime, heavy repair costs and potential for fatality. Approximately half of all rotating machine failures are due to issues with the roller bearings making early detection of defects a high priority [1]. Bearing damage can also lead to performance degradation, excessive vibration, noise and damage to other components if left unchecked. This makes online condition monitoring highly desirable so potential issues can be detected and rectified during scheduled maintenance. Common defects include galling, spalling, brinelling, peeling, wear, fatigue, overloading, particle ingress and lack of lubrication [2, 3]. Depending on where the defect occurs it can excite one of the four characteristic fault frequencies: ball pass frequency outer (BPFO), ball pass frequency inner (BPFI), ball spin frequency (BSF) and fundamental train frequency (FTF) [1, 4]. Determined by the bearing geometry and rotational speed, these frequencies, described in Equations (1) – (4), manifest in both vibration and acoustic signals, detectable with appropriate processing techniques, albeit in different frequency ranges.

$$BPFO = \frac{nf_r}{2}\left[1 - \frac{d}{D}\cos\Phi\right] \quad (1)$$

$$BPFI = \frac{nf_r}{2}\left[1 + \frac{d}{D}\cos\Phi\right] \quad (2)$$

$$BSF = f_r\frac{D}{2d}\left[1 - \left(\frac{d}{D}\cos\Phi\right)^2\right] \quad (3)$$

$$FTF = \frac{f_r}{2}\left[1 - \frac{d}{D}\cos\Phi\right] \quad (4)$$

where f_r is the shaft speed, n is the number of rollers, Φ is the angle of load from the radial plane, d is the ball diameter, and D is the pitch diameter - under conditions of no slippage.

The frequency and amplitude of such defects provides an indication of the presence and severity of the defect with harmonics indicating the defect origin [1]. It is important to recognise that in the case of a point defect, such frequencies are related to how often there is a defect impact and characteristics will manifest at different frequencies in the audio and vibration frequency spectrums.

For bearing fault classification, physical vibration sensing methods are well established, but advances in computational technology and signal processing techniques have allowed acoustic methods to be developed, with associated advantages viz. being remote to the equipment means acoustic sensors can be setup more easily, quickly and safely and are not prone to the same issues of vibration or heat damage as with surface mounted sensors; acoustic measurements are able to detect faults at an earlier stage in their emergence; the acoustic signal is likely to contain more defect information such as size and position and should give greater accuracy than vibration measurements [1, 2, 5, 6, 7].

Acoustics have been well established as promising for fault detection and condition monitoring with research being active for at least 2 decades [1, 2]. However, only relatively recently have significant advancements been made compared to earlier studies through use of advanced computational hardware, signal processing tools and machine learning techniques [2, 6, 8]. Furthermore, the uptake of acoustic techniques has been slow due to a historic knowledge, confidence in, and reliance on, direct vibration sensing systems; with acoustic techniques remaining in their relative infancy with regard to widespread

familiarity and industry expertise [2, 6]. This paper aims to demonstrate the potential simplicity of using acoustic technology whilst showing that low-cost and readily available devices are able to be employed. Therefore, this paper presents an investigation into the use of smartphones and consumer-grade microphones for acoustically detecting faults on roller element bearings using Fourier transform feature extraction and multi-SVM classification.

A. *Traditional Acoustic Fault Detection Methods*

In [7], experimental results from acoustic and vibration signals for seeded defects on the outer race of roller bearings are compared in an effort to identify the defect type and estimate its size. The test facility employed a piezoelectric Physical Acoustic WD sensor (100 – 1000 kHz) and a resonant accelerometer (flat frequency response between 0.01 – 8 kHz – Model 236 Isobase); sampling rates ranged between 2 – 10 MHz. Despite not performing any pre-processing, they were able to detect and estimate the size of protrusions on the outer race. Results from vibration measurements were unable to detect early defects or discern any further information. Another study, [9], investigated low speed bearing fault diagnosis using both vibration and acoustic signals and comparing the performance of a relevance vector machine and a SVM. For data collection, a micro-DSP system was created using PCI board with 18-bit, 10 MHz A/D conversion and onboard processing sampling at 500 kHz. The signal was supplied by a Physical Acoustics R3a AE sensor with a frequency range of 25 – 530 kHz. Pre-processing was by independent component analysis using the top five components as input features. Again, the authors found the acoustic signal to give superior classification accuracy to the vibration sensor measurements, more so when using the relevance vector machine over the SVM. The authors of [10] present a hybrid signal processing technique combining ensemble empirical mode decomposition with multiscale principal component analysis for detecting incipient faults in large-size low-speed roller bearings. Four specialised Valpey-Fisher VP-1093 pinducers with a frequency response of 0.001 – 10 MHz were used – these are designed for shock wave applications. This method is general in nature allowing it to be applied to a wide range of problems; it demonstrated its efficacy using both acoustic and vibration measurements, particularly with non-stationary signals. The work presented in [11] employs a wavelet packet transform on an acoustic signal for fault detection and size estimation in roller bearings. The AE frequency range for faults were identified as 100 kHz to 1 MHz and a Nano-30 Physical Acoustic sensor (good frequency response from 125 – 750 kHz) was used being sampled at 2 MHz for 5 seconds. Plackett-Burman Experimental Design determined the most sensitive parameter from ring down counts, peak value, rms, kurtosis, burst duration, crest factor and skewness. Wavelet coefficients were calculated utilizing DMeyer, Daubechies, Symlets, and Coiflets orthogonal mother wavelet families to investigate which wavelet function maximizes its Kurtosis to Shannon Entropy ratio. Using the continuous wavelet transform and Kurtosis to Shannon Entropy ratio as quantitative measurements the optimal mother wavelets for signal decomposition were chosen. After applying the wavelet packet transform, the signal envelope in different frequency bands was calculated using the Hilbert-transform. This method delivers excellent fault detection, specialising in extracting weak impulse-like fault features heavily masked by noise. In [12], acoustic signals were analysed using Hilbert-Huang transform for feature extraction and an asymmetric proximity function and k - nearest neighbour hybrid classification algorithm. The authors of [13] looked at acoustic and vibration signals, processing using an adaptive line enhancer and high-frequency resonance technique. They used a Physical Acoustics R15 sensor with a frequency response of 150 kHz connected directly to an ALM8 processor which outputs a demodulated version similar to that processed with high-frequency resonance. The work of [14] used a Physical Acoustics D9201A sensor with a 20 – 90 kHz band-pass filter and 8-bit 200 kHz A/D conversion. Signal processing was by high frequency resonance, finding better performance using a short-time overlapping energy technique – similar to the method to be used in this paper. Several studies [9, 10], have identified the limitations of acoustic techniques; requiring high frequency (over 100 kHz) response and data acquisition using specialised hardware; sampling between 1 and 5 MHz. Low speed applications require longer recording durations to capture the mechanical defect frequencies giving high data storage and processing demands. Consequently, acoustic data is often analysed in the hit-based or continuous time spectrum and rarely in the frequency spectrum.

This work uses readily accessible equipment sensitive in the audible frequency range with much lower sampling rates to record acoustic fingerprints of different bearing faults; investigating the suitability for fault diagnosis.

B. *Classification & Machine Learning Algorithms*

The performance of any classification algorithm is highly dependent on the differentiating features presented for training. Several studies [15, 16, 17], have compared the performance of SVMs and ANNs for bearing fault classification and concluded that SVMs outperform their counterpart with regard to accuracy, training time and computational efficiency. The authors of [15] compared SVMs with ANNs, optimising their parameters using genetic algorithms and finding the ANN to require significantly more training time. Both systems were capable of 100% accuracy, but the SVM was significantly quicker. In [16], results from two classification methods are compared; a radial basis kernel SVM optimised for the cost and gamma parameters to use the minimum number of support vectors, and a three-layer feed-forward artificial neural network trained using supervised back propagation. Results indicated that the SVM is more readily implemented, and gave better results. SVMs tends to perform better than ANNs for this application, but only for smaller datasets [17]. Note that implementation on real industrial machines would require a much larger and more sophisticated data set in which case ANNs would likely give better performance. Based on these findings, in this study a multi-SVM classification learner is employed; negating the effects of different operating conditions by training a new SVM for each operational regime.

II. METHODOLOGY

In this section, details of the experimental setup used to capture runtime data are given followed by the signal processing and machine learning techniques used to analyse the data.

A. Experimental Setup & Data Acquisition

A Gunt PT501 bearing fault simulator consists of an electric drive motor, shaft with laser tachometer, and bearing housing with interchangeable bearings. The bearing housing vibration is monitored using a built in single-axis accelerometer mounted vertically. The housing is horizontally loaded by winding a micrometre screw onto a rubber compression spring mounted to the housing edge. A control unit provides power to the motor for a user defined speed setting. The vibration accelerometer is connected to a OWON VDS3102 USB oscilloscope allowing remote sampling using a laptop. Microphone audio measurements are sampled using two Audio-Technica AT2020 USB+ condenser cardioid microphones. These are setup in stereo equidistant from and facing the bearing housing. The experimental setup is shown in Fig. 1. The seeded bearing defects under study are shown in Fig. 2. Smartphone audio is sampled using a Samsung Galaxy S7 Edge placed ≈ 20 cm away with the microphone facing the bearing. This is an intuitively sensible positon based on operational ease and optimum sound pressure level; closer causes overload of the sensor during louder operating regimes and further away permits greater signal attenuation. The smartphone position was not fixed in keeping with real-world practical operation.

Table I summarises the experimental setup and equipment used. Data is recorded for each combination of speed, load and bearing resulting in 24 different operating conditions ($6\ speeds \times 4\ loads$) and 144 different setups ($24\ operating\ conditions \times 6\ bearings$). The speed setting correlates linearly with the actual shaft rpm and are listed at no load (as loading the bearing reduces the rpm by approximately 1 to 2 rpm per mm). The load also correlates linearly, with load being applied from approximately 3.8 mm, with settings 4, 5 and 6 mm corresponding approximately to 5, 18 and 32 N respectively.

B. Signal Processing & Classification

Fig. 3 gives an overview of the signal processing methodology. For each setup, measurements are imported into Matlab and the time signal extracted. The data is divided into training and testing datasets for the SVM; using the first 4 datasets for training and a fifth for testing. The smartphone dataset signals are divided into two 4-second signals; one for training and one for testing. The audio signals are clipped to 8 seconds from the middle removing unwanted artefacts from the beginning and end of the recording. To create a sufficient number of observations each signal is divided into ten 1-second overlapping observations. Although it is possible to increase the classification accuracy by increasing the number of observations, it impacts computational time. Fig. 4 shows a time plot of the smartphone audio for one of the observations. Frequency responses are calculated for each observation sample using a Fast Fourier Transform. Fig. 5 shows example frequency responses for the same observation. It can be seen that the energy content of the signal is primarily contained in the 0 – 5,000 Hz range for the acoustic data and 0 – 16,000 Hz for the vibration data (not shown). Within these ranges, peaks above a set threshold are extracted. The threshold is calculated for each operating condition based on bearing A as the mean plus the standard deviation (1σ was found to be optimal). The frequency ranges specified above are then divided into bins and the peaks in each bin obtained. Fig. 6 shows the peaks above the threshold, the bin edges and the mean of the frequency plot.

Three features are calculated for the SVM: the total number of peaks above the threshold within the specified frequency range, the number of peaks in each bin and the product of the amplitude of the peaks in each bin. The frequency range for each bin is fixed at 100 Hz, giving 50 bins for the acoustic frequency range and 160 for the vibration. This gives a total number of SVM input features as 101 (total number of peaks, count of peaks in each bin and product of peaks in each bin) for acoustic and 321 for the vibration. The data is then rearranged for input into the SVM, with features representing columns and observations representing rows in the input table.

For each operating condition (speed and load combination) a quadratic SVM (2^{nd} order polynomial kernel function) is trained using a box constraint of 1, and without standardisation of the data. By using a different SVM for each operating condition, inaccuracies due to changes of the speed and load are eliminated allowing the SVM to differentiate exclusively between the bearings. This is reasonable for real-world machinery as operating settings will be known. Evaluation of SVM accuracy is by k-fold cross-validation using 5 non-overlapping folds; this splits the observations into folds and trains with the out-of-fold observations and validates using the in-fold observations and then calculates the average error over all folds. Note that the cross-validation is only performed on the training dataset for the purpose of preventing under and over fitting and increasing SVM robustness.

For system testing, the exact same processing is carried out on the testing data. The respective SVM for each operating condition is used with the associated test data input. Finally, modal recombination recombines the observations into an overall response for each input signal. As there are 10 observations per signal, a majority of 6 identical responses is required.

There are a number of limitations to this methodology. The signals used in this case are all under steady-state conditions – real world applications will exhibit both transients and dynamic stability. However, this method could be easily expanded to include dynamic signals, alternatively a larger dataset would allow accurate interpolation between the support vectors which should provide a reasonable response. This method does not address online condition monitoring, the aim being to detect faults as they form and monitor their growth allowing maximum use before planned maintenance is required. Moreover, only a limited number and type of defect are used.

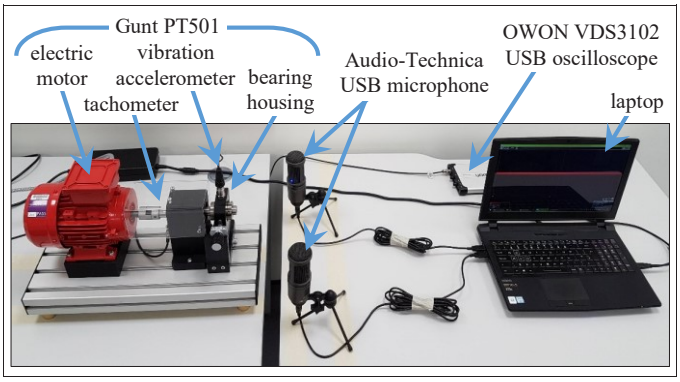

Fig. 1. Experimental setup showing; the Gunt PT501, two USB microphones, the OWON oscilloscope, and the laptop. The smartphone position is not shown as it varied, however, it was placed roughly between the two microphones at about the same height as the bearing.

Fig. 2. Damaged bearings from left to right; bearing C showing the inner race defect, bearing E showing the roller defect and bearing F showing wear. Note there was only a single defect on the inner race of bearing E compared to the two defects seen above on bearing C.

TABLE I. EXPERIMENTAL PROCEDURE

Setting		Description		
Bearings NU 204 E TVP2; 12 rollers at 7.5 mm diameter & 34 mm pitch diameter	**A**	New bearing with no damage (reference bearing)		
	B	Damage to outer race		
	C	Damage to inner race		
	D	Damage to roller element		
	E	Damage to outer race, inner race and roller element		
	F	Heavily worn bearing		
Speed Setting & Equivalent Speed		Setting: 0 → 298 rpm		
		Setting: 2 → 829 rpm		
		Setting: 4 → 1341 rpm		
		Setting: 6 → 1865 rpm		
		Setting: 8 → 2428 rpm		
		Setting: 10 → 3050 rpm		
Load Settings		3, 4, 5 and 6 mm		
		Smartphone	**Microphone**	**Vibration**
Sampling software & format		Android Voice Recorder: mp3 @160 kbps	Matlab: Matlab file	OWON VDS_S2: text file
Sampling rate		44,100 Hz	48,000 Hz	100,000 Hz
A/D resolution		8-bit	16-bit	8-bit
Sensor frequency response		Unknown	20 to 20,000 Hz	1 to 10,000 Hz
Sensitivity		Unknown	-19dB ± 4 (audio circuit)	100 mV/g & 1V/division
Repeats		1	5	5
All recordings were single channel and of 10 second duration.				

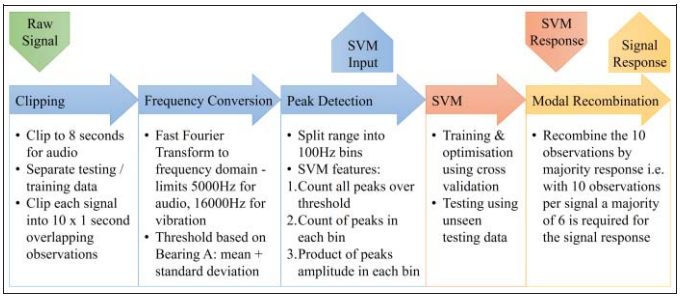

Fig. 3. Signal processing methodology.

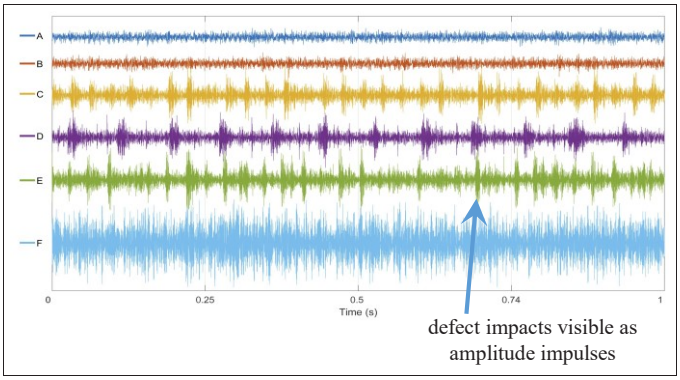

Fig. 4. Smartphone audio one second time plot for all bearings at speed 6 and load 5. Note the clearly visible audio spikes visible for bearings C and D; inner race and roller defects respectively.

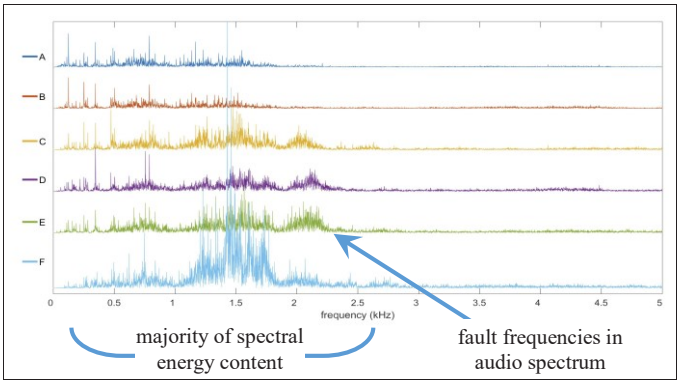

Fig. 5. Smartphone frequency plot for all bearings at speed 6 and load 5. Note the differences from that of bearing A are primarily related to the defects present and characterise the fault frequencies in the audio frequency spectrum. However, there will also be small differences caused by tiny changes in operating conditions, setup, etc.

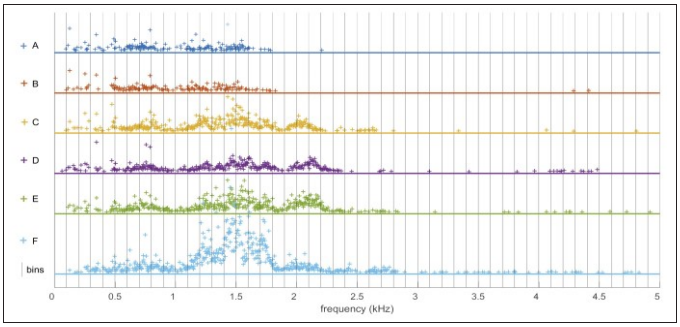

Fig. 6. Smartphone peaks plot for all bearings at speed 6 and load 5. Vertical lines represent bin boundaries, and the horizontal line shows the mean of each signal. Note the cut off threshold was the mean plus one standard deviation.

III. Experimental Results

Table II shows the cross validation classification accuracy from the training data averaged across all operating conditions, it is clear the system performs very well. Table III shows the classification accuracy from the testing data categorised by bearing, speed and load. The values are a percentage of correct classification across all the observations. Table IV shows the count of the misclassified signals after all the observations have been regrouped using modal recombination. It can be seen that with modal recombination the accuracy is increased further. Furthermore, it highlights where misclassifications occur most. For the smartphone data this is at low loads with a total of 6 misclassifications out of 144 inputs; 4 and 2 of those at load settings 3 and 4 mm respectively.

For the microphone data, regrouping the observations gives perfect classification, but examining the signal majorities revealed that the performance is only just good enough to achieve this. Whilst the vibration accuracy has increased to 75% it still exhibits some misclassifications, particularly between bearings A and B. This is likely due to the outer race fault not producing sufficiently strong vibrations to allow differentiation. At a load setting of 6 mm the vibrations are sufficient to significantly increase the classification accuracy.

The results clearly show significantly greater classification accuracy of the acoustic signals compared with the vibration measurements. Fig. 7 shows that as the speed increases the classification accuracy is better for both acoustic and vibration signals. It is notable that the sound level indicator displayed during recording with the smartphone was at its maximum value for speed settings 8 and 10 when load was applied. This might be a cause for the degradation in accuracy for the smartphone results compared to the microphone, and if so could be rectified by positioning the smartphone further away reducing the sound pressure to within its most sensitive range. Fig. 8 shows greater classification accuracy as the load increases. The acoustic performance is increasingly better than vibration at low loads and speeds. Fig. 9 shows that bearing E was the most difficult to classify. This is expected as it exhibits the combined faults of bearings B, C and D. Examining the misclassifications reveals they are usually attributed to bearings B, C, or D i.e. a fault is still detected as it not misclassified as a healthy bearing. Clearly the most important differentiation is between a healthy and unhealthy bearing state; bearing A and the other five bearings. This is where the acoustic method outperformed the vibration with no misclassifications; compared to the vibration with 7 unhealthy signals classified as healthy and 9 healthy signals classified as unhealthy (out of 144 inputs).

There is sufficient information in the acoustic signals to detect the faults under all operating conditions, particularly at low load and speed, where the vibration only started to achieve reasonable performance at high load. Moreover, there are no misclassifications between healthy and unhealthy bearings with the acoustic signals, whereas approximately 5% of vibration signals are misclassified as healthy.

TABLE II. Multi-SVM Training Data Cross Validation Accuracy

	Smartphone	Microphone	Vibration
Mean Accuracy (%)	99.97	99.97	99.75
Standard Deviation	0.02	0.03	0.01

TABLE III. Observation Classification Results (%)

		Smartphone	Microphone	Vibration
Bearing	**A**	96.25	95.83	63.75
	B	95.83	96.25	57.08
	C	87.50	95.83	82.08
	D	97.08	93.75	72.50
	E	90.83	95.00	68.33
	F	95.42	99.58	85.83
Speed Setting	**0**	90.42	90.83	50.42
	2	93.75	97.08	75.00
	4	93.75	97.08	72.92
	6	97.92	95.42	81.25
	8	91.67	97.08	75.42
	10	95.42	98.75	74.58
Load Setting (mm)	**3**	86.67	92.78	65.00
	4	94.17	95.28	68.89
	5	97.22	97.78	69.72
	6	97.22	98.33	82.78
Overall Accuracy (%)		**93.82**	**96.04**	**71.60**

TABLE IV. Grouped Signal Error Count

		Smartphone	Microphone	Vibration
Bearing	**A**	0	0	7
	B	0	0	10
	C	2	0	4
	D	0	0	6
	E	2	0	5
	F	2	0	3
Speed Setting	**0**	1	0	11
	2	1	0	3
	4	1	0	7
	6	0	0	3
	8	2	0	4
	10	1	0	7
Load Setting (mm)	**3**	4	0	10
	4	2	0	13
	5	0	0	9
	6	0	0	3
Total Misclassified		6	0	35
Overall Accuracy (%)		**95.83**	**100**	**75.69**

TABLE V. Motor Control Classification Results

	Smartphone	Microphone
Overall Accuracy (%)	**97.50**	**100**

The ability of the smartphone and microphone to outperform the vibration signal not only demonstrates the efficacy of acoustics but also the suitability of this type of consumer equipment for bearing fault diagnosis and similar applications. Whilst for real applications the training database and processing requirements exceed the capabilities of smartphones, these devices are suitable for data acquisition which can then be uploaded for processing to then deliver the classification result.

The use of multi-SVM classification based on the operating conditions lead to a significant increase in the classification accuracy and was just as easy to program. This method of programming can be easily expanded to allow interpolation for dynamic signals. When classifying between bearings, the ability to differentiate exclusively between them without inaccuracies caused by different operating conditions is one of the main contributing factors to the high classification accuracies achieved.

IV. Extension to Motor Control System Diagnostics

The case studies have been extended to include consideration of current controller dynamics. Unstable current dynamics in brushless pulse modulation machines, for instance, is a relatively common issue under widely varying operational conditions or when commissioning controllers. In the most severe circumstances, inappropriately controlled currents can lead to permanent demagnetisation of the motor as well as damage of the power electronics. A brushless dc motor is setup, controlled using a digital PWM current controller with a 10kHz PWM frequency. The current controller is known to exhibit transient instability under some operating conditions creating high frequency torque transients. The smartphone and audio microphones are used to sample audio under two operating conditions both healthy and unhealthy states. The smartphone records 3 samples of 10 seconds, and the microphones record 5 samples of 3 seconds. The signals are processed exactly as previously discussed. Table V shows the results – with only a single observation misclassification with the smartphone (based on 40 observation inputs. Fig. 10 shows a current instability captured using an oscilloscope. The acoustic setup was easily transferred to a different machine for this investigation, whereas the vibration probe could not be transferred to a different machine without considerable work and high risk of damage.

V. Conclusion

This paper set out to demonstrate the potential simplicity of acoustic bearing fault detection compared with previous works and compare results with vibration measurements. The setup and method is proven to deliver extremely good classification accuracy with easy to setup independent sensors and reduced computational demands. The multi-SVM approach was shown to be extremely effective for allowing differentiation exclusively between the bearings. The method also shows great applicability to motor control system diagnostics. The suitability of consumer audio recording tools opens up bearing fault diagnosis to a much wider audience with improved cost/benefit performance.

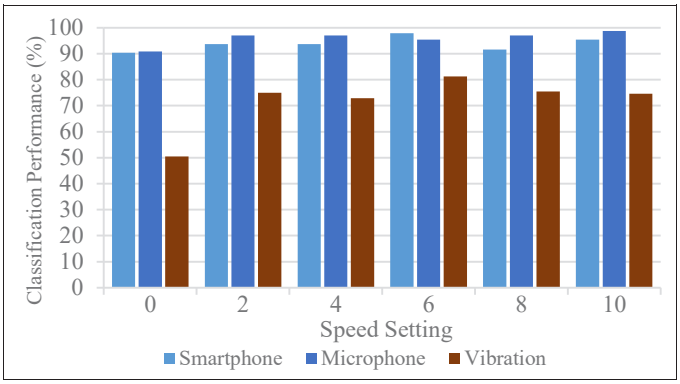

Fig. 7. Speed setting classification performance based on Table III.

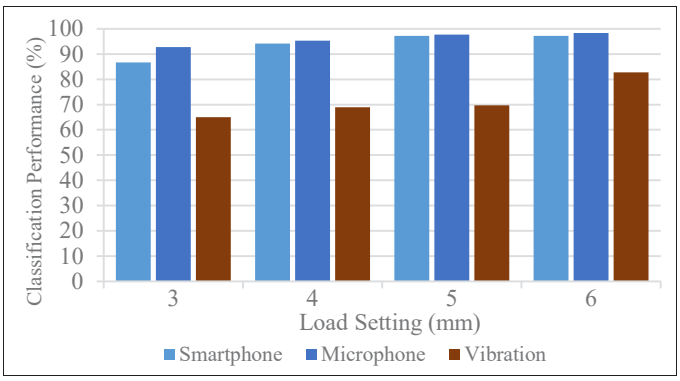

Fig. 8. Load setting classification performance based on Table III.

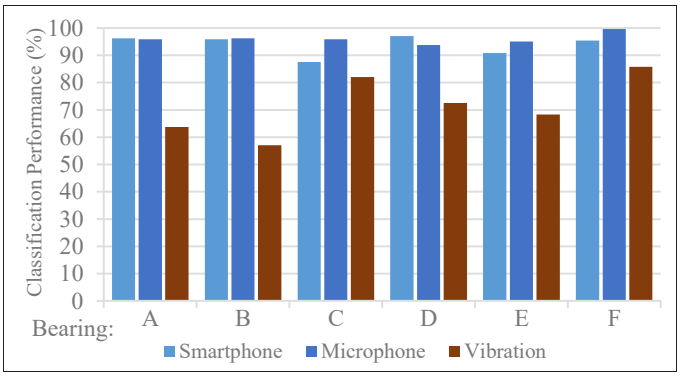

Fig. 9. Bearing classification performance based on Table III.

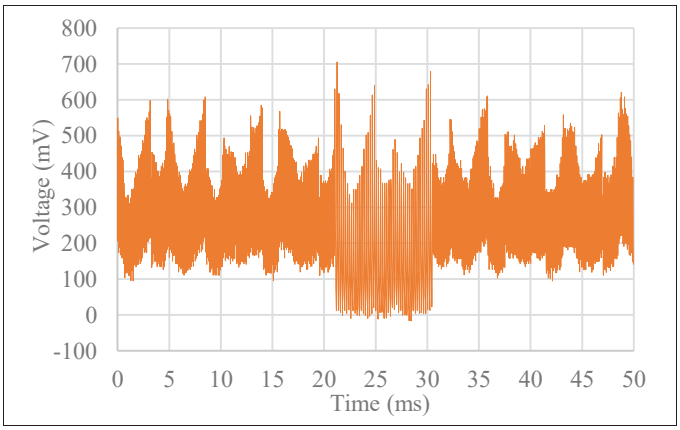

Fig. 10. Oscilloscope save showing motor PWM current – instability visible between 21 and 31 milliseconds.

ACKNOWLEDGMENTS

The author would like to thank Damiano Rossetti who assisted with the SVM coding, and Pierre Francq who assisted in the optimisation of the system.

REFERENCES

[1] A. Rai and S. H. Upadhyay, "A review on signal processing techniques utilized in the fault diagnosis of rolling element bearings," *Tribology International,* vol. 96, pp. 289-306, 2016.

[2] N. Tandon and A. Choudhury, "A review of vibration and acoustic measurement methods for the detection of defects in rolling element bearings," *Tribology International,* vol. 32, no. 8, p. 469–480, 1999.

[3] M. Entezami, E. Stewart, J. Tutcher, W. Driscoll, R. Ellis, G. Yeo, Z. Zhang, C. Roberts, T. Kono and S. Bayram, "Acoustic analysis techniques for condition monitoring of roller bearings," *Railway Condition Monitoring, 6th Conference 2014,* pp. 1-8, 2014.

[4] S. A. McInerny and Y. Dai, "Basic vibration signal processing for bearing fault detection," *IEEE Transactions On Education,* vol. 46, no. 1, pp. 149-156, 2003.

[5] H. Li, F. Xu, H. Liu and X. Zhang, "Incipient fault information determination for rolling element bearing based on synchronous averaging reassigned wavelet scalogram," *Measurement,* vol. 65, pp. 1 - 10, 2015.

[6] D. Mba and R. B. K. N. Rao, "Development of acoustic emission technology for condition monitoring and diagnosis of rotating machines; bearings, pumps, gearboxes, engines and rotating structures," *The Shock and Vibration Digest,* vol. 38, no. 1, pp. 3 - 16, 2006.

[7] A. M. Al-Ghamd and D. Mba, "A comparative experimental study on the use of acoustic emission and vibration analysis for bearing defect identification and estimation of defect size," *Mechanical Systems and Signal Processing,* vol. 20, no. 7, p. 1537–1571, 2006.

[8] X. Lou and K. A. Loparo, "Bearing fault diagnosis based on wavelet transform and fuzzy inference," *Mechanical Systems and Signal Processing,* vol. 18, no. 5, pp. 1077 - 1095, 2004.

[9] A. Widodoa, E. Y. Kimb, J.-D. Sonc, B.-S. Yangc, A. C. C. Tanb, D.-S. Gud, B.-K. Choid and J. Mathewb, "Fault diagnosis of low speed bearing based on relevance vector machine and support vector machine," *Expert Systems with Applications,* vol. 36, no. 3, pp. 7252 - 7261, 2009.

[10] M. Žvokelj, S. Zupan and I. Prebil, "Multivariate and multiscale monitoring of large-size low-speed bearings using ensemble empirical mode decomposition method combined with principal component analysis," *Mechanical Systems and Signal Processing,* vol. 24, no. 4, pp. 1049 - 1067, 2010.

[11] F. Hemmati, W. Orfali and M. S. Gadala, "Roller bearing acoustic signature extraction by wavelet packet transform, applications in fault detection and size estimation," *Applied Acoustics,* vol. 104, p. 101–118, 2016.

[12] D. H. Pandya, S. H. Upadhyay and S. P. Harsha, "Fault diagnosis of rolling element bearing with intrinsic mode function of acoustic emission data using APF-KNN," *Expert Systems with Applications,* vol. 40, no. 10, pp. 4137 - 4145, 2013.

[13] J. Shiroishi, Y. Li, S. Liang, T. Kurfess and S. Danyluk, "Bearing condition diagnostics via vibration and acoustic emission measurements," *Mechanical Systems and Signal Processing,* vol. 11, no. 5, pp. 693 - 705, 1997.

[14] C. James Li and S. Y. Li, "Acoustic emission analysis for bearing condition monitoring," *Wear,* vol. 185, no. 1 - 2, pp. 67 - 74, 1995.

[15] B. Samanta, K. R. Al-Balushi and S. A. Al-Araimi, "Artificial neural networks and support vector machines with genetic algorithm for bearing fault detection," *Engineering Applications of Artificial Intelligence,* vol. 16, no. 7 - 8, pp. 657 - 665, 2003.

[16] P. Konar and P. Chattopadhyay, "Bearing fault detection of induction motor using wavelet and support vector machines (SVMs)," *Applied Soft Computing,* vol. 11, no. 6, pp. 4203-4211, 2011.

[17] Y. Yang, D. Yu and J. Cheng, "A fault diagnosis approach for roller bearing based on IMF envelope spectrum and SVM," *Measurement,* vol. 40, no. 9 - 10, pp. 943 - 950, 2007.

[18] K. Feng, Z. Jiang, W. He and Q. Qin, "Rolling element bearing fault detection based on optimal antisymmetric real Laplace wavelet," *Measurement,* vol. 44, no. 9, pp. 1582-1591, 2011.

[19] W. He, Z.-N. Jiang and K. Feng, "Bearing fault detection based on optimal wavelet filter and sparse code shrinkage," *Measurement,* vol. 42, no. 7, pp. 1092 - 1102, 2009.